

Some recent advances in understanding the mineralogy of Earth's deep mantle

BY THOMAS S. DUFFY*

Department of Geosciences, Princeton University, Princeton, NJ 08544, USA

Understanding planetary structure and evolution requires a detailed knowledge of the properties of geological materials under the conditions of deep planetary interiors. Experiments under the extreme pressure–temperature conditions of the deep mantle are challenging, and many fundamental properties remain poorly constrained or are inferred only through uncertain extrapolations from lower pressure–temperature states. Nevertheless, the last several years have witnessed a number of new developments in this area, and a broad overview of the current understanding of the Earth's lower mantle is presented here. Some recent experimental and theoretical advances related to the lowermost mantle are highlighted. Measurements of the equation of state and deformation behaviour of $(\text{Mg},\text{Fe})\text{SiO}_3$ in the CaIrO_3 -type (post-perovskite) structure yield insights into the nature of the core–mantle boundary region. Theoretical studies of the behaviour of MgSiO_3 liquids under high pressure–temperature conditions provide constraints on melt volumes, diffusivities and viscosities that are relevant to understanding both the early Earth (e.g. deep magma oceans) and seismic structure observed in the present Earth (e.g. ultra-low-velocity zones).

Keywords: mantle; post-perovskite; silicate liquids; Earth interior; MgSiO_3

1. Introduction

Knowledge of the composition and structure of the Earth's deep mantle places important constraints on the processes involved in the Earth's formation and subsequent evolution. Our understanding of the Earth's deep interior is derived from several lines of evidence including geophysical observations (e.g. seismology), geochemical studies of natural rocks and minerals, numerical simulations of mantle dynamics and experimental and theoretical studies of the physical and chemical properties of Earth materials at high pressures and temperatures. In this work, a basic overview of our understanding of the mantle structure is given. This is followed by more detailed discussion of selected recent research related to the Earth's core–mantle boundary region and the properties of silicate liquids under deep Earth conditions.

Experimental capabilities for studying materials at extreme conditions are progressing rapidly. Advances in X-ray diffraction methods at synchrotron radiation facilities have expanded the P – T range accessible to direct

*duffy@princeton.edu

One contribution of 14 to a Discussion Meeting Issue 'Origin and differentiation of the Earth: past to present'.

measurements all the way up to 200 GPa and 3000 K, while, at the same time, leading to improved resolution that has resulted in dramatically better ability to recover physical and crystallographic properties (Duffy 2005). *Ab initio* theoretical studies have also made major strides in the size and scope of problems that can be addressed (Gillan *et al.* 2006). In combination with new geophysical observations of the Earth, we can now better address such fundamental questions as the origin of seismic discontinuities, chemical heterogeneity in the mantle and the nature of the core–mantle boundary region.

2. Overview of the Earth's mantle

The most detailed information about the structure of the Earth comes from analysis of seismic waves generated by earthquakes. From such studies, one-dimensional models of compressional and shear velocity with depth can be constructed for either specific regions or a global average (Kennett *et al.* 1995). The mantle is characterized by major seismic velocity discontinuities at 410 and 660 km depths and an anomalously steep velocity gradient in the transition zone between them. The uppermost mantle (above 300 km) shows strong regional variations in velocity and also exhibits considerable seismic anisotropy, especially in the upper 200 km.

The Earth's lower mantle, extending from 660 km to a depth of approximately 2900 km, is the single largest region of the Earth, containing roughly 100 times the mass of the Earth's crust. In contrast to the upper mantle, seismic profiles for the lower mantle reveal generally smooth increases in seismic velocity with depth. However, the region that lies just above the core–mantle boundary, known for historical reasons as D'', is one that exhibits significant heterogeneity and anomalous properties (Garnero 2000).

Over the last 20 years, seismologists have progressed in constraining the three-dimensional seismic structure in the mantle using seismic tomography (Romanowicz 1991). Tomographic studies are able to resolve the velocity variations associated with subducting lithospheric plates and thereby image their interaction with the 660 km seismic discontinuity. More recently, tomographic studies have examined the nature of rising plumes of hot material (hotspots; Montelli *et al.* 2004). The velocity variations imaged by tomography can mostly be ascribed to the effects of temperature (Duffy & Ahrens 1992b; Karato 1993; Karato & Karki 2001), but chemistry and phase may also be important, especially in regions such as the subcontinental lithosphere and the deepest mantle.

A key question is the extent to which the mantle is compositionally uniform or whether large-scale heterogeneities or compositionally distinct regions exist. Some geochemical evidence from analysis of the distribution of trace elements and radiogenic isotopes in different rock types favours the existence of long-lived chemically isolated reservoirs, perhaps associated with major seismic discontinuities (van Keken *et al.* 2002). However, evidence from seismic tomography suggests that many subducting lithospheric slabs penetrate through the 660 km discontinuity, although some slabs are impeded or deflected by the boundary (van der Hilst *et al.* 1997). This suggests that the 660 km discontinuity does not isolate the upper and lower mantle into compositionally distinct regions. There is seismic evidence of chemical heterogeneity in the deep mantle (Kellogg *et al.* 1999;

van der Hilst & Karason 1999). It has therefore been suggested that the bottom third of the mantle may be geochemically distinct, and more heterogeneous, although no global sharp discontinuity in seismic velocity has been detected there (Kellogg *et al.* 1999). While polymorphism of the major lower mantle phases is not expected until the D'' region, changes in the spin state of Fe in $(\text{Mg},\text{Fe})\text{O}$ and $(\text{Mg},\text{Fe})\text{SiO}_3$ have been detected experimentally at relevant pressures (Badro *et al.* 2003), and these may have profound implications for understanding the bottom third or so of the mantle.

The chemistry of the Earth's mantle is inferred from petrological data supplemented by constraints on the bulk chemical composition of the Earth. Direct samples of the uppermost mantle provide constraints on the chemistry of the upper 200 km or so of the Earth's mantle. Less direct constraints come from the study of basalts that are derived from the upper mantle by partial melting at mid-ocean ridges. Mineral inclusions in diamond (Stachel *et al.* 2000; McCammon 2001) provide rare samples of the deeper mantle, perhaps even to the depths of the transition zone or lower mantle. Interpretation of all these samples is augmented by constraints on the Earth's bulk chemistry (McDonough & Sun 1995) largely derived from the estimation of Solar System chemical abundances (from measurements of the solar photosphere and primitive meteorites).

The overall picture that results is that the uppermost mantle is composed of a Fe- and Mg-rich rock type (pyrolite), which upon partial melting produces the basalts of the oceanic crust and the residual peridotite of the depleted uppermost mantle (Irifune & Tsuchiya 2007). Determining whether the composition of deeper regions matches that of the uppermost mantle is one of the major challenges of mineral physics research. In the upper mantle, a pyrolite composition produces four primary minerals: olivine ($(\text{Mg},\text{Fe})_2\text{SiO}_4$); orthopyroxene ($(\text{Mg},\text{Fe})\text{SiO}_3$); clinopyroxene ($\text{CaMgSi}_2\text{O}_6$); and pyrope-rich garnet ($(\text{Mg},\text{Fe},\text{Ca})_3\text{Al}_2\text{Si}_3\text{O}_{12}$). Olivine is the dominant upper mantle mineral component in this model (approx. 60% by volume). Support for the model comes from the fact that, at the expected temperatures of the mantle, phase transformations in olivine occur at pressures corresponding roughly to those at depths of 410 and 660 km, the major seismic discontinuities of the upper mantle. This is a basis for expecting that the bulk chemical composition inferred from near-surface rocks may extend across the entire upper mantle, and perhaps through the Earth's mantle as a whole. However, there is also evidence that the fraction of olivine needed to satisfy seismic data in the transition zone is significantly below that of the pyrolite model (Duffy *et al.* 1995; Cammarano & Romanowicz 2007). Furthermore, the presence of phase transitions does not rule out the existence of chemical changes as well (Jeanloz 1991).

The four mineral components of pyrolite ultimately transform to assemblages that are dominated by perovskite-structured phases. These transformations occur at depths corresponding to the transition zone and the vicinity of the 660 km discontinuity. Thus, from a mineralogical viewpoint, the 660 km discontinuity plays a central role in the Earth's mantle owing to the emergence of six-coordinated, perovskite-dominated assemblages.

Experimental studies have shown that the mineral assemblage adopted by a peridotite or pyrolite lithology under lower mantle conditions consists of three main minerals: $(\text{Mg},\text{Fe})\text{SiO}_3$ perovskite; CaSiO_3 perovskite; and $(\text{Mg},\text{Fe})\text{O}$ ferropericlase (Ringwood 1991; Kesson *et al.* 1998; Lee *et al.* 2004;

Ono & Oganov 2005; Irifune & Tsuchiya 2007). In peridotite compositions, aluminium is incorporated into the perovskite structures, but, in more Al_2O_3 -rich systems such as basalt, a separate Al-rich phase as well as a SiO_2 phase is expected to be present (Irifune & Ringwood 1993; Hirose *et al.* 1999; Funamori *et al.* 2000).

3. Post-perovskite and the core–mantle boundary region

The D'' region is one of the most poorly understood parts of the planet. A seismic discontinuity marks the top of D'' and the region itself is characterized by strong lateral heterogeneity and other anomalous properties (Garnero 2000; Lay & Garnero 2007). In contrast to the bulk of the lower mantle, the core–mantle boundary region exhibits pronounced seismic anisotropy (Kendall 2000). Local regions of much reduced (more than 10%) seismic velocities (ultra-low-velocity zones, ULVZs) have also been observed. These have been attributed to partial melting at the base of the mantle (Williams & Garnero 1996). They might also arise from iron enrichment due to either chemical interactions between the mantle and the core or other causes (Mao *et al.* 2004; Dobson & Brodholt 2005; Stackhouse *et al.* 2006). Complexity in the deepest mantle should not be surprising given that it is the boundary between the silicate minerals of the mantle and the liquid iron alloy of the core. The region is also a likely source area for mantle plumes (Montelli *et al.* 2004) and a potential final repository for subducting slabs of plate tectonics. Strong temperature gradients are also expected across D'' as it represents the thermal boundary layer between the mantle and the core.

The recent discovery (Murakami *et al.* 2004; Oganov & Ono 2004) of a post-perovskite (pPv) phase (CaIrO_3 -type structure) in MgSiO_3 at 125 GPa, close to conditions expected for the D'' region, has major potential implications for understanding geophysics and geochemistry of the deep mantle. The orthorhombic CaIrO_3 -type phase consists of edge- and corner-sharing SiO_6 octahedra that form layers along the (010) plane. The octahedral sheets alternate with eightfold coordinated magnesium layers along the *b* crystallographic axis. The structure is anisotropic with the highest compressibility normal to layering. The new phase contrasts markedly with the perovskite structure, which consists of a three-dimensional network of corner-linked SiO_6 octahedra with eightfold coordinated Mg filling in the cavities on this framework.

Although our understanding of this phase transition and its implications is still at an early stage, the CaIrO_3 -type phase of $(\text{Mg}, \text{Fe})\text{SiO}_3$ appears to provide some of the right characteristics to match seismic observations of D'' (Wookey *et al.* 2005; Lay & Garnero 2007; Shim 2008). While there remain considerable uncertainties in laboratory pressure determinations at these extreme conditions, the transformation occurs at pressures near those found at the top of the D'' layer for expected mantle compositions (Murakami *et al.* 2004; Oganov & Ono 2004; Wookey *et al.* 2005). The strongly positive pressure–temperature or Clapeyron slope of the transition means that the observed topography of the D'' boundary is explained by a deeper transition in locally hotter regions and a shallower transition in cooler regions (Hirose 2006). This is consistent with the seismic observation which suggested that a phase transition with a strong, positive

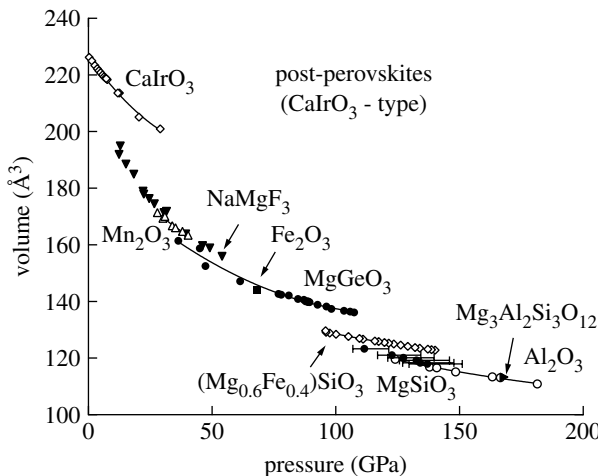


Figure 1. Representative volume–pressure relations for compounds in the post-perovskite (CaIrO_3 -type) structure. Solid lines are simple polynomial fits to the data (Oganov & Ono 2004; Ono & Ohishi 2005; Tateno *et al.* 2005; Kubo *et al.* 2006; Mao *et al.* 2006; Martin *et al.* 2006, 2007; Ono *et al.* 2006; Santillan *et al.* 2006; Hustoft *et al.* 2008).

Clapeyron slope (approx. 6 MPa K⁻¹) could explain the topography of the D'' discontinuity (Sidorin *et al.* 1999). In addition, the Earth has a steep thermal gradient near the core–mantle boundary and temperatures at the base of the mantle may become sufficiently hot that perovskite may re-emerge just above the core (Hernlund *et al.* 2005). In this case, one may expect complex structures such as localized lens of pPv. Attempts to seismically image these structures in this region have already yielded some provocative results (Lay *et al.* 2006; van der Hilst *et al.* 2007; Hutko *et al.* 2008).

A large number of compounds have now been discovered to possess the pPv structure, mostly at elevated pressures (figure 1). Owing to the high synthesis pressures required to form silicate pPvs, many experiments of interest cannot readily be performed on this material. Analogue compositions can therefore be useful by allowing measurements to be carried out at lower pressures. For example, germanates have long been known to be good structural analogues for silicates with corresponding phase transitions occurring at low pressures in germanates (Ringwood & Seabrook 1963). The pPv phase transition in MgGeO_3 occurs near 55–70 GPa (Hirose *et al.* 2005; Tsuchiya & Tsuchiya 2007a), compared with approximately 125 GPa in MgSiO_3 . Other materials found to crystallize in the pPv structure include various sesquioxides (Fe_2O_3 , Al_2O_3 and Mn_2O_3) and NaMgF_3 . pPv is the stable phase of CaIrO_3 at ambient conditions.

(a) Equation of state of $(\text{Mg}, \text{Fe})\text{SiO}_3$ pPv

The equation of state (EOS) is one of the most fundamental parameters obtained from high-pressure studies. Using the laser-heated diamond anvil cell, the equations of state of coexisting perovskite and pPv (CaIrO_3 -type) have been investigated using phases synthesized from a natural pyroxene composition with a $\text{Fe}/(\text{Fe} + \text{Mg})$ value of 0.09, close to that expected for the lower mantle (Shieh *et al.* 2006). The measured pressure–volume data for the pPv phase from 12 to

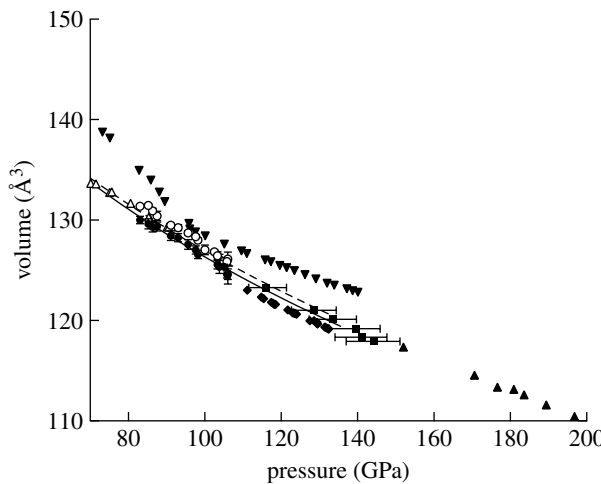


Figure 2. Selected pressure–volume compression data for perovskite (open triangles (dashed line), En100 (Fiquet *et al.* 2000); open circles, En91Fs09 (Shieh *et al.* 2006)) and CaIrO₃-type (filled squares, En100 (Ono *et al.* 2006); filled diamonds, En100 (Guignot *et al.* 2007); filled circles (solid line), En91Fs09 (Shieh *et al.* 2006); filled down triangles, En60Fs40 (Mao *et al.* 2006); filled up triangles, En85Co15 (Kubo *et al.* 2007)) phases at 300 K. En, enstatite (MgSiO₃); Fs, ferrosilite (FeSiO₃); Co, corundum (Al₂O₃). For the En100 data of Ono *et al.* (2006), pressure error bars show uncertainty in pressure depending on the choice of three different scales for the gold pressure calibrant. Also shown are representative volume error bars for a selected study (Shieh *et al.* 2006). Solid line is a Birch–Murnaghan EOS fit to the CaIrO₃-type data of Shieh *et al.* (2006) for the En91Fs09 composition. The dashed line is the EOS for MgSiO₃ perovskite (Fiquet *et al.* 2000).

106 GPa yield a zero-pressure bulk modulus of 219(5) GPa and a zero-pressure volume of 164.9(6) Å³ when $K'_0 = 4$ (figure 2). From the fitted EOS, the variation of the bulk modulus with compression can be determined (figure 3). The bulk modulus of pPv is 575(15) GPa at a pressure of 100 GPa. These results are broadly consistent with theoretical calculations (Oganov & Ono 2004) and other experimental EOS studies of (Mg,Fe)SiO₃ pPv (Ono *et al.* 2006; Guignot *et al.* 2007; Shim *et al.* 2008).

A direct comparison of volumes of coexisting perovskite and CaIrO₃-type phases at 80–106 GPa demonstrates that the pPv phase has a smaller volume than perovskite by 1.1(2) per cent (figure 2). Using measured volumes together with the bulk modulus calculated from EOS fits, we find that the bulk sound velocity decreases by 2.3(2.1) per cent across this transition at 120 GPa (figure 3), which is again consistent with theoretical predictions. Because the shear wave velocity is expected to increase across the transition, the decrease in bulk sound velocity implies that perovskite–CaIrO₃-type transition should produce a stronger shear wave signal in comparison with compressional waves. This is consistent with seismic studies that report a 2–3 per cent increase in V_S across the transition while the increase in V_P is usually smaller or even undetectable (Lay *et al.* 2006; Hutko *et al.* 2008). Quenched samples from these experiments (Shieh *et al.* 2006) were analysed by transmission electron microscopy. It was found that crystalline perovskite grains are enriched in iron ($Mg/(Mg+Fe)=0.89$) compared with adjacent amorphous parts ($Mg/(Mg+Fe)=0.93$) presumably converted from pPv (Hirose *et al.* *in press*). This

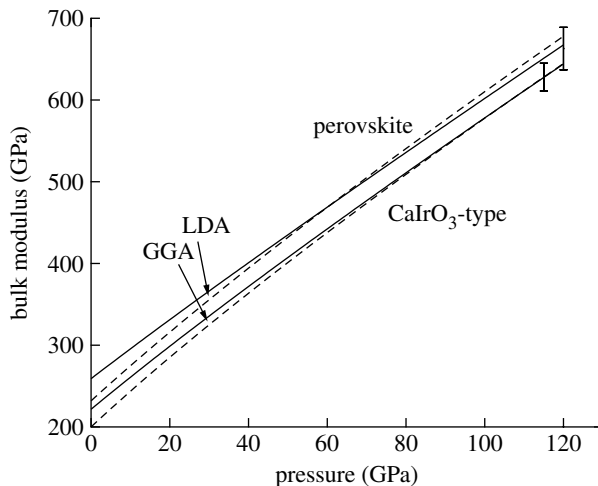


Figure 3. Bulk moduli of Fe-bearing perovskite and CaIrO₃-type post-perovskite calculated from EOS fits (Shieh *et al.* 2006) and compared with density functional theory calculations for MgSiO₃ (Oganov & Ono 2004).

indicates that ferrous iron stabilizes perovskite to higher pressures. Simultaneous volume measurements of the perovskite and pPv forms of MgSiO₃ have also recently been reported by Komabayashi *et al.* (2008).

In another recent study, experiments using glass starting materials with compositions along the MgSiO₃ (En)–Al₂O₃ (Co) join have recently been carried out to investigate the effects of Al content on the EOS, transformation pressure and stability limits of the new phase (Kubo *et al.* 2007). The pPv phase was synthesized for compositions with 0, 5, 15 and 20 mol% corundum at pressures above 120 GPa. The effect of Al₂O₃ incorporation is to increase the transition pressure and lead to the formation of a potentially broad two-phase coexistence region containing perovskite and pPv. Sensitivity of the phase transition pressure and thickness to compositional variables such as FeO and Al₂O₃ may also contribute to D'' boundary topography. Determining the width of the coexistence region is challenging due to potential metastability and sluggish reaction kinetics. However, for the En₈₅Co₁₅ composition, the perovskite and pPv phases were observed to coexist between 127 and 152 GPa. The increases in transition pressure and width of the mixed phase region are qualitatively consistent with theory (Akber-Knutson *et al.* 2005). Dissolution of Al₂O₃ into MgSiO₃ pPv also appears to have a major effect on the pressure–volume relationship (figure 2), which is again consistent with theoretical predictions (Caracas & Cohen 2005; Stackhouse *et al.* 2005a).

(b) Deformation studies of germanate and silicate post-perovskites

One of the most interesting properties of the D'' region is that it possesses relatively strong (and variable) seismic anisotropy (Kendall 2000; Lay & Garnero 2007). The velocities of horizontally polarized shear waves (V_{SH}) are approximately 3 per cent faster than vertically polarized shear waves (V_{SV}) in some well-studied regions such as the circum-Pacific. The anisotropy, however,

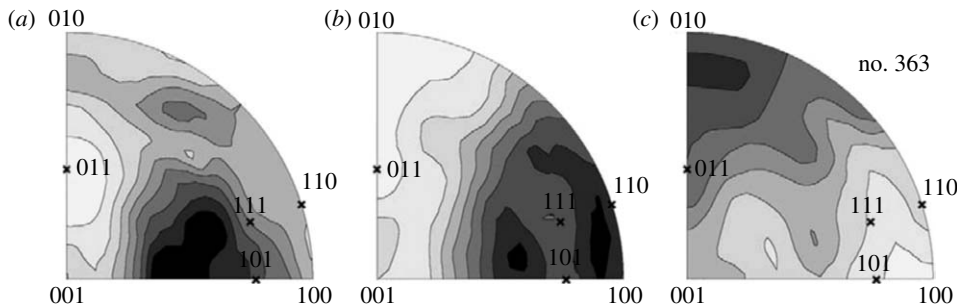


Figure 4. Inverse pole figures from deformation experiments on CaIrO_3 -type post-perovskites with compositions (a) $(\text{Mg},\text{Fe})\text{SiO}_3$ (157 GPa, 300 K; [Merkel et al. 2007](#)), (b) MgGeO_3 (130 GPa, 300 K; [Merkel et al. 2006](#)) and (c) CaIrO_3 (6 GPa, 800 K; [Miyagi et al. 2008](#)). MgGeO_3 and $(\text{Mg},\text{Fe})\text{SiO}_3$ post-perovskites are best explained by dominant slip on the (100) and (110) planes, while CaIrO_3 itself is best explained by slip on (010)[100]. Adapted from [Miyagi et al. \(2008\)](#).

is complex and varies from region to region. Understanding seismic anisotropy can yield clues to mantle dynamics at the base of the mantle. However, interpretation of seismic anisotropy in the deep Earth is challenging as it requires an understanding of mineral deformation mechanisms, the anisotropic elastic properties of the relevant phases and the strain history of materials in the deep mantle.

Measurement of the deformation behaviour of silicate pPv within its pressure–temperature stability field is not possible at present. However, using the diamond anvil cell and X-ray diffraction measurements in a radial geometry ([Duffy et al. 1999](#)), the deformation behaviours of MgGeO_3 and MgSiO_3 pPvs have been constrained at room temperature and pressures of 104–157 GPa, a pressure range directly relevant to the deep mantle ([Merkel et al. 2006, 2007](#)). Figure 4 shows inverse pole figures from these deformation experiments, showing the distribution of crystal planes relative to the loading axis of the diamond anvil cell. For both the silicate and germanate pPvs, polycrystalline plasticity simulations were performed and show that the observed textures can be explained by deformation with (110) and (100) as the primary slip planes. These results are consistent with a recent theoretical study, which found that slip along (110) could produce a series of stacking fault structures between perovskite and pPv and proposed that such planes were likely candidates for slip planes in CaIrO_3 -type pPv ([Oganov et al. 2005](#)).

Plastic strains in pPv and the corresponding contribution to seismic anisotropy in D'' were calculated using mantle convection models, polycrystalline plasticity simulations and constraints on the anisotropic elastic moduli of CaIrO_3 -type MgSiO_3 under D'' conditions ([Merkel et al. 2007](#)). The shear wave anisotropy pattern that results from this model is highly variable with azimuth, and the fast polarization direction is generally inclined to the vertical. Horizontally polarized shear waves are typically slower than vertically polarized shear waves, in contrast to many seismic observations.

There are several possible explanations that may be able to reconcile the deformation experiments with seismic observations. The elastic moduli of CaIrO_3 -type $(\text{Mg},\text{Fe})\text{SiO}_3$ under deep mantle conditions remain uncertain as available

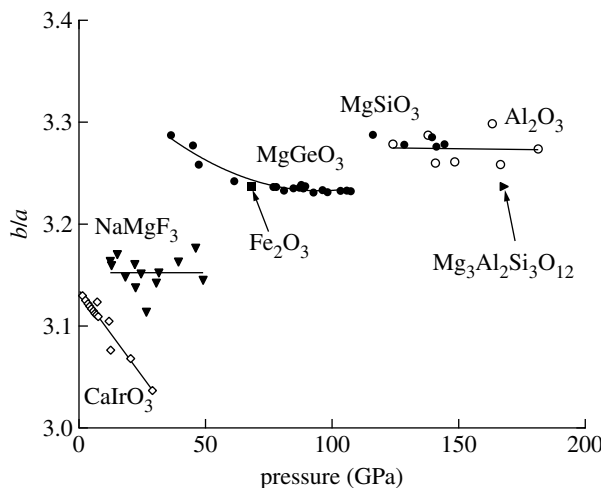


Figure 5. Crystallographic b/a ratio for selected post-perovskites from figure 1. Lines are least-squares fits.

theoretical calculations at high P - T conditions show significant differences (Stackhouse *et al.* 2005b; Wentzcovitch *et al.* 2006). A detailed analysis of the anisotropy patterns resulting from various combinations of slip systems and sets of elastic constants can be found elsewhere (Stackhouse & Brodholt 2007). Other phases such as (Mg,Fe)O are also highly anisotropic under D'' conditions and may contribute to or even dominate the seismic anisotropy signal even if they are not the volumetrically most abundant phase (Long *et al.* 2006). Another possibility is that high-temperature deformation mechanisms in (Mg,Fe)SiO₃ are different from the measured room-temperature values, or the experimental textures observed in (Mg,Fe)SiO₃ and MgGeO₃ are textures that result from a phase transformation rather than deformational textures (Santillan *et al.* 2006).

Based on the layered nature of the crystal structure of the CaIrO₃-type phase, it has been suggested that (010) slip (i.e. parallel to the octahedral sheets) may instead be a likely deformation mechanism for this structure. A number of deformation experiments have been performed at relatively low pressures and high temperatures on the analogue material CaIrO₃ pPv (Miyajima *et al.* 2006; Yamazaki *et al.* 2006; Walte *et al.* 2007; Miyagi *et al.* 2008), and these consistently find that, indeed, [100](010) slip is the dominant slip mechanism at both room temperature and high temperatures. Theoretical studies have provided support for both (110) slip and (010) slip in MgSiO₃ pPv (Oganov *et al.* 2005; Carrez *et al.* 2007). Some modelling studies have suggested that [100](010) slip could provide a plausible explanation for observations of lowermost mantle seismic anisotropy (Yamazaki *et al.* 2006).

A key question in evaluating the results for MgGeO₃ and CaIrO₃ pPvs is whether these materials represent good analogues for the silicate (figure 1). The relevance of an analogue material can be tested by examining a range of structural properties (axial ratios, compressibility, bond distances, polyhedral distortions, etc.) in the analogue and the real material. Figure 5 shows a comparison of crystallographic b/a ratios for different compositions in the CaIrO₃-type structure. Silicates, germanates and sesquioxides exhibit similar b/a

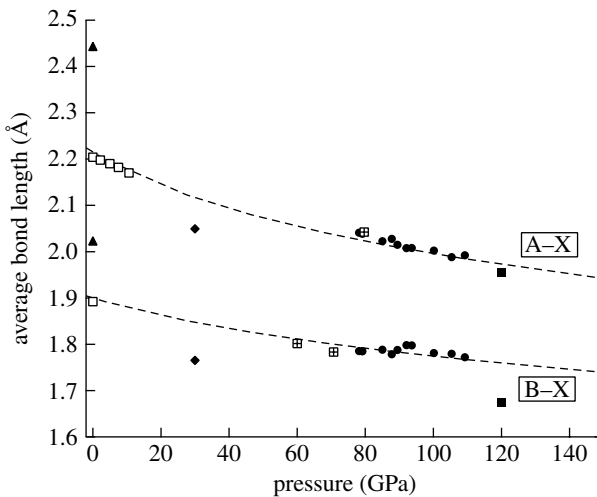


Figure 6. Average bond lengths from single-crystal X-ray diffraction, powder X-ray diffraction analysed by the Rietveld method and theoretical studies of ABX_3 post-perovskites and other phases. Filled circles indicate experimental data (Rietveld method) for MgGeO_3 (Kubo *et al.* 2008). Dashed line shows the results of 0 K theoretical calculations for MgGeO_3 (Kubo *et al.* 2008). Filled squares, MgSiO_3 post-perovskite at 120 GPa (theory; Tsuchiya *et al.* 2004); filled diamonds, NaMgF_3 pPv at 30 GPa (theory; Umemoto *et al.* 2006); filled triangles; single-crystal X-ray diffraction for CaIrO_3 pPv at ambient conditions (experiment; Rodi & Babel 1965); open squares, single-crystal X-ray diffraction for MgSiO_3 and CaGeO_3 perovskites (Sasaki *et al.* 1983; Ross & Hazen 1990); squares with plus, powder X-ray diffraction (Rietveld method) for $\alpha\text{-PbO}_2$ -type GeO_2 and MgSiO_3 perovskite (Fiquet *et al.* 2000; Prakapenka *et al.* 2003; Shiraki *et al.* 2003).

ratios but the value for CaIrO_3 is considerably lower than that for the other materials. Rietveld structure refinements of X-ray diffraction data and/or density functional theory (DFT) calculations can be used to evaluate atomic-level structural parameters such as bond distances, angles and polyhedral volumes and distortion. A comparison of various structural parameters for diffraction studies of MgGeO_3 , MgSiO_3 , NaMgF_3 and CaIrO_3 pPvs has been reported (Kubo *et al.* 2008). This study found some similarities between MgSiO_3 and MgGeO_3 pPvs in axial ratios, averaged Mg–O distance, MgO_8 polyhedral volume and degree of octahedral distortion as well as consistency in elastic systematics and generally similar behaviour in axial compressibilities. Surprisingly, the NaMgF_3 pPv phase shows even closer similarities in structural parameters with MgSiO_3 pPv. As one example, figure 6 shows average A–X and B–X bond distances for these ABX_3 pPvs. Both MgGeO_3 and NaMgF_3 possess average distances similar to MgSiO_3 , whereas CaIrO_3 differs markedly with considerably longer bond distances for both polyhedral sites. Considerable differences between the elastic properties of CaIrO_3 and MgSiO_3 have also been reported from theoretical calculations (Tsuchiya & Tsuchiya 2007b). Consideration of all these differences raises serious questions about the relevance of measurements on CaIrO_3 for understanding silicate pPvs. Further studies are needed to evaluate whether the deformational properties of this compound can be used reliably to make inferences about the behaviour of the corresponding silicate under deep Earth conditions.

4. MgO–SiO₂ liquids at deep mantle pressures

(a) Deep mantle melting

Melting is a ubiquitous process during early planetary evolution and a primary mechanism of planetary differentiation. The properties of silicate liquids are thus essential for understanding a wide range of geophysical phenomena related to the deep Earth and its origin and evolution. Energy deposited into the growing Earth by impacting planetesimals is likely to have produced strong heating and the presence of magma oceans at or below the Earth's surface during accretion appears inevitable (Tonks & Melosh 1993). There is evidence that early magma oceans were prevalent on Mars, the Moon and even many asteroids (Warren 1985; Righter & Drake 1996; Greenwood *et al.* 2005). On Earth, the subsequent cooling and crystallization of a magma ocean might have led to the chemical differentiation of the mantle (Ohtani 1985). Understanding the dynamics of a terrestrial magma ocean is essential to understand the initial conditions for the thermal and chemical evolution of the Earth (Tonks & Melosh 1993; Labrosse *et al.* 2007). The liquid viscosity and its depth dependence are among the important parameters that characterize an early (liquid-rich) magma ocean (Solomatov 2000). Viscosity controls the thermal state and dynamic processes in the magma ocean and influences its subsequent evolution and crystallization (Solomatov 2000). In the present mantle, partial melting may explain the ULVZs found in the D'' layer near the core–mantle boundary (Williams *et al.* 1998; Lay *et al.* 2004). Small degrees of partial melt distributed throughout the lower mantle could also provide an explanation for the high relative values of seismic shear anomalies compared with compressional anomalies (Duffy & Ahrens 1992a). Gravitationally stable partial melt layers have also been proposed in the upper mantle such as atop the 410 km discontinuity (Revenaugh & Sipkin 1994; Song *et al.* 2004; Matsukage *et al.* 2005), and this could help explain the geochemical differences between basalts from mid-ocean ridges and those from island arcs (Bercovici & Karato 2003).

One key question about melting in the deep Earth involves the density contrast between the solid and the melt. The buoyancy of the melt relative to the coexisting solid will be controlled by the molar volume change on melting, as well as compositional differences (i.e. Fe enrichment) between the melt and the solid. Enhanced compressibility of melts relative to solids can lead to density crossovers under mantle *P*–*T* conditions. Densities of silicate liquids have been studied using shock wave techniques (Rigden *et al.* 1984; Miller *et al.* 1991; Mosenfelder *et al.* 2007) or by sink–float methods in multi-anvil apparatus (Agee & Walker 1993; Ohtani & Maeda 2001; Agee 2008), and density inversions between silicate melts and equilibrium liquidus crystals have been identified (Rigden *et al.* 1984; Agee 1998). However, there are few constraints on possible density inversions under conditions of the Earth's lower mantle. While it has been proposed based on laboratory measurements to 15 GPa that basaltic melts may become denser than mantle peridotite at conditions near the base of the mantle (Ohtani & Maeda 2001), these results are subject to considerable uncertainty due to the long extrapolation involved. The existence of a dense magma ocean near the base of the mantle early in Earth's history could provide a means to generate the geochemical heterogeneities observed in the present-day mantle (Labrosse *et al.* 2007).

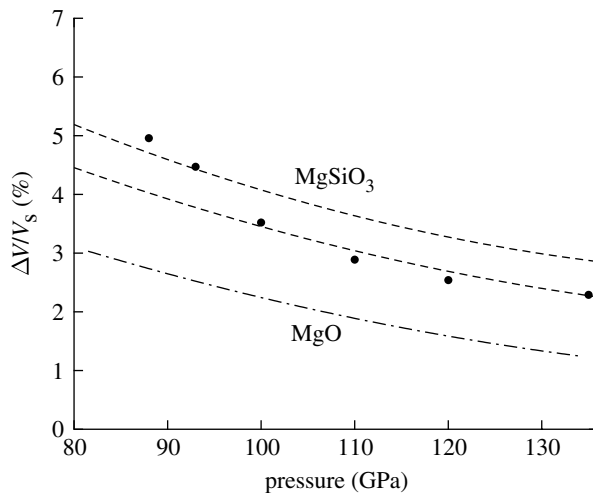


Figure 7. Molar volume difference between the liquid and the solid normalized to molar volume of the solid for MgSiO_3 and MgO liquids from recent first-principles simulations. For MgSiO_3 , circles are from Wan *et al.* (2007) and correspond to 3500 K; dashed curves are from Stixrude & Karki (2005) for 3000 and 4000 K, respectively. Results for MgO (dot-dashed curve) are from Karki *et al.* (2006b).

Experimental studies of silicate liquids at deep mantle pressures are challenging. An alternative approach to the study of high-pressure liquid properties is to use computer simulations. Molecular dynamics (MD) simulations using semi-empirical intermolecular potentials have been used to compute densities and other properties of silicate melts (Wasserman *et al.* 1993; Lacks *et al.* 2007). These have the advantage that the semi-empirical potentials allow for long simulation times that are important for constraining transport properties. However, the reliability of the potentials used at high P and T must be evaluated carefully.

Recently, several studies (Stixrude & Karki 2005; Karki *et al.* 2006a,b; Wan *et al.* 2007; de Koker *et al.* 2008) have reported simulations of the properties of liquid silicates at deep mantle pressures using *ab initio* molecular dynamics simulations and DFT (Car & Parrinello 1985). These simulations allow for theoretical study from the first principles, i.e. without empirical or adjustable parameters of the properties of solid and liquid silicates at arbitrary conditions of pressure and temperature. DFT, in the local density approximation (LDA), or with its generalized gradient approximation (GGA) improvements, is the most advanced theoretical tool to predict the microscopic properties of materials. While many DFT studies have focused on static (zero-temperature) properties such as crystal structures and low-temperature elastic constants, it is now possible to carry out sufficient long runs at high temperatures using molecular dynamics to compute the required thermal averages necessary to obtain the structural and dynamic properties of high-temperature silicate liquids. For example, one recent simulation on MgSiO_3 liquid carried out runs for approximately 10 ps on a system containing 80 atoms (16 MgSiO_3 units; Wan *et al.* 2007).

Figure 7 compares the results of recent *ab initio* simulations of liquid MgSiO_3 and MgO . The plot shows the difference, ΔV , between the liquid molar volume, V_L , and the solid molar volume, V_S , normalized to the volume of the solid as a

function of pressure at 85–135 GPa. Temperatures in these simulations were between 3000 and 4000 K, and the pressures correspond to depths from approximately 1950 km to the core–mantle boundary. For both MgO and MgSiO₃, the volume difference between the liquid and the solid decreases with depth owing to the higher compressibility of the liquid than the solid. At 3500 K and 88 GPa, the density of crystalline MgSiO₃ in the perovskite structure is 5 per cent greater than liquid MgSiO₃, whereas the density excess is reduced to 2.9 per cent at 120 GPa and 5000 K (Wan *et al.* 2007). The absolute volumes calculated for liquid or solid MgSiO₃ are approximately 3–4 per cent different in the two recent studies (Stixrude & Karki 2005; Wan *et al.* 2007), and this is mostly due to the different approximations (LDA versus GGA) used in the DFT. The volume or density differences between the liquid and the solid are more directly comparable since both phases are calculated using the same DFT approximations.

The *ab initio* simulations to date for MgSiO₃ indicate that volumes of liquid MgSiO₃ remain 2–3 per cent greater than those of solid perovskite up to D'' conditions (Stixrude & Karki 2005; Wan *et al.* 2007). The transformation to a pPv structure is expected to further reduce the solid volume by 1–1.5 per cent (Oganov & Ono 2004; Shieh *et al.* 2006). For MgO, the volume excess of the liquid is approximately 1 per cent at the core–mantle boundary. A density crossover in MgSiO₃ relative to perovskite densities is not expected to occur until 180 GPa, and this would be even higher relative to pPv (Wan *et al.* 2007). These results imply that density crossovers due solely to the enhanced compressibility of the liquid relative to the solid are not expected for these compositions in the MgO–SiO₂ system. However, the convergence of solid and liquid volumes and densities with pressure will make it more plausible that chemical differences between the melt and the solid can lead to neutral or negatively buoyant liquids in the deep Earth. Fe is known to partition preferentially into the melt. Estimates of the solid–liquid partition coefficients for Fe needed to achieve neutral buoyancy in (Mg,Fe)SiO₃ compositions appear to be plausible based on very limited experimental data at lower mantle conditions (Wan *et al.* 2007).

Recent shock experiments on Mg₂SiO₄ forsterite and wadsleyite starting materials have been interpreted as producing melts that are denser than the corresponding solids (MgSiO₃ pPv and MgO) by 3.7 ± 3.0 per cent at 142 GPa and by 2.2 ± 1.8 per cent at 151 GPa, respectively, along the Hugoniot (Mosenfelder *et al.* 2007). These experimental results do not appear consistent with the molecular dynamics simulations discussed above, and further work is needed to understand these differences.

(b) Diffusivity and viscosity of MgO–SiO₂ liquids

Molecular dynamics simulations of liquid properties using either *ab initio* methods or semi-empirical potentials allow for determination of diffusivities from the mean-square displacements of the ions. Diffusivities control chemical reaction rates and are relevant to phenomena such as magma mixing, and crystal growth and dissolution. As with molar volumes, *ab initio* calculations provide insights into liquid behaviour over a much wider range of conditions that can be studied with current laboratory techniques alone.

Table 1. Diffusivities of selected oxide and silicate liquids from theory and experiment.

	P (GPa)	T (K)	D ($\text{cm}^2 \text{s}^{-1}$)	reference
<i>experiment</i>				
CaMgSi ₂ O ₆	15	2573	9.1×10^{-6}	Reid <i>et al.</i> (2003)
<i>theory</i>				
MgSiO ₃	5	4500–5000	$2\text{--}4 \times 10^{-5}$ (Si,O), $7\text{--}10 \times 10^{-6}$ (Mg)	Wasserman <i>et al.</i> (1993)
MgSiO ₃	47	3000	$2\text{--}3 \times 10^{-6}$ (Si,O), 7.3×10^{-6} (Mg)	Lacks <i>et al.</i> (2007)
MgSiO ₃	120	4000	4.6×10^{-6}	Wan <i>et al.</i> (2007)
MgSiO ₃	120	5000	3.3×10^{-5}	Wan <i>et al.</i> (2007)
MgO	19	3000	5.0×10^{-5} (O), 9.2×10^{-5} (Mg)	Lacks <i>et al.</i> (2007)
MgO	20	3000	$2\text{--}4 \times 10^{-5}$	Karki <i>et al.</i> (2006a)
MgO	105	3000	$1.5\text{--}6.5 \times 10^{-6}$	Karki <i>et al.</i> (2006a)
MgO	121	5000	$2\text{--}3 \times 10^{-5}$	Karki <i>et al.</i> (2006a)

Table 1 compares diffusivities of selected mantle-relevant compositions (CaMgSi₂O₆, MgSiO₃ and MgO) from experiment and theory over a range of P – T conditions. Comparison of data using different techniques and over different P – T ranges must be approached with caution. Nevertheless, a broad picture of the behaviour of diffusivities in these simple liquid systems is beginning to emerge from theoretical calculations. Results above 1 Mbar for both MgSiO₃ and MgO indicate that the temperature dependence of diffusivity remains strong at deep mantle conditions as a temperature change of 1000 K produces approximately an order of magnitude change in diffusivity (Karki *et al.* 2006a; Wan *et al.* 2007). This is a consequence of a stronger pressure dependence of diffusivity at lower temperatures (e.g. 3000 K) than at higher temperatures (e.g. 5000 K) (Karki *et al.* 2006a). Secondly, the diffusivities in MgSiO₃ and MgO liquids are broadly similar at these deep conditions. At approximately 120 GPa and 4000 K, the diffusivities range from approximately $5 \times 10^{-5} \text{ cm}^2 \text{s}^{-1}$ decreasing to $2\text{--}3 \times 10^{-5} \text{ cm}^2 \text{s}^{-1}$ at the same pressure and 5000 K (Karki *et al.* 2006a; Wan *et al.* 2007).

A direct comparison of empirical potentials and *ab initio* results can be made at approximately 19 GPa and 3000 K for MgO (Karki *et al.* 2006a; Lacks *et al.* 2007). Under these conditions, Karki *et al.* (2006a) obtained diffusivities of approximately $2\text{--}4 \times 10^{-5} \text{ cm}^2 \text{s}^{-1}$ compared with values of $5 \times 10^{-5} \text{ cm}^2 \text{s}^{-1}$ (for O) and $9 \times 10^{-5} \text{ cm}^2 \text{s}^{-1}$ (for Mg) from the empirical calculations, which indicate that the MD simulations using empirical potentials are producing diffusivities about twice as large as the *ab initio* simulations. A direct comparison of theory and experiment is not possible at present. The *ab initio* simulations on diopside-composition liquids would be useful in order to compare theory more directly with experiments (Reid *et al.* 2001) and to constrain the pressure dependence of diffusivity in this system.

The viscosities of silicate liquids control melt transport. Estimates of viscosities can be obtained from mean diffusion coefficients from the Debye–Stokes–Einstein formula or Eyring equation. Viscosities of oxide and silicate liquids from experiment are compared with *ab initio* and semi-empirical molecular dynamics in table 2. Estimated viscosities in MgSiO₃ liquids at D''

Table 2. Viscosities of silicate liquids from theory and experiment.

	P (GPa)	T (K)	η (Pa s)	reference
<i>experiment</i>				
CaMgSi ₂ O ₆	8–13	2200–2470	0.028–0.51	Reid <i>et al.</i> (2003)
peridotite	3–13	2041–2523	0.019–0.13	Liebske <i>et al.</i> (2005)
peridotite	10 ^{−4}	1850	0.126	Dingwell <i>et al.</i> (2004)
<i>theory</i>				
peridotite	10 ^{−4}	5000	3×10 ^{−4}	Dingwell <i>et al.</i> (2004)
MgSiO ₃	14	3000	0.013	Lacks <i>et al.</i> (2007)
MgSiO ₃	47	3000	0.178	Lacks <i>et al.</i> (2007)
MgSiO ₃	120	4500–5000	0.019–0.031	Wan <i>et al.</i> (2007)

conditions (120 GPa, 4000–5000 K) are broadly similar to values obtained at low pressures (approx. 10 GPa, 2400 K) from falling sphere experiments on a peridotite liquid and from empirical MD simulations (at approx. 14 GPa, 3000 K) on MgSiO₃ liquids (Liebske *et al.* 2005; Lacks *et al.* 2007). To the extent that these results are comparable, this implies that pressure and temperature effects are of roughly equal importance in controlling how viscosity changes at great depth. It may be that viscosities in the deep mantle are similar to values in the shallow mantle because the competing effects of pressure and temperature roughly balance. However, changes in melt structure with P and T mean that the viscosity may behave non-monotonically with depth. Again, *ab initio* calculations can yield important insights into how properties such as the coordination number vary over a wide range of P – T conditions (Stixrude & Karki 2005).

The use of theoretical molecular dynamics simulations to study silicate liquids in the deep Earth is still in its infancy. Nevertheless, the promise of the method has been demonstrated. Improvements in experimental methods have also been rapid, but it is not likely that experiments will approach conditions of the Earth's deep mantle in the near future. However, it is important that the theoretical calculations be tested and benchmarked by comparison with experimental studies at lower P – T conditions.

This work was supported by the NSF and the Carnegie–DOE Alliance Center. Synchrotron X-ray diffraction experiments were carried out at the GSECARS and HPCAT sectors of the Advanced Photon Source.

References

- Agee, C. B. 1998 Crystal–liquid density inversions in terrestrial and lunar magmas. *Phys. Earth Planet. Inter.* **107**, 63–74. ([doi:10.1016/S0031-9201\(97\)00124-6](https://doi.org/10.1016/S0031-9201(97)00124-6))
- Agee, C. B. 2008 Static compression of hydrous silicate melt and the effect of water on planetary differentiation. *Earth Planet. Sci. Lett.* **265**, 641–654. ([doi:10.1016/j.epsl.2007.11.010](https://doi.org/10.1016/j.epsl.2007.11.010))
- Agee, C. B. & Walker, D. 1993 Olivine flotation in mantle melt. *Earth Planet. Sci. Lett.* **114**, 315–324. ([doi:10.1016/0012-821X\(93\)90033-6](https://doi.org/10.1016/0012-821X(93)90033-6))
- Akber-Knutson, S., Steinle-Neumann, G. & Asimow, P. D. 2005 Effect of Al on the sharpness of the MgSiO₃ perovskite to post-perovskite phase transition. *Geophys. Res. Lett.* **32**, L14 303. ([doi:10.1029/2005GL023192](https://doi.org/10.1029/2005GL023192))

- Badro, J., Fiquet, G., Guyot, F., Rueff, J. P., Struzhkin, V. V., Vanko, G. & Monaco, G. 2003 Iron partitioning in Earth's mantle: toward a deep lower mantle discontinuity. *Science* **300**, 789–791. ([doi:10.1126/science.1081311](https://doi.org/10.1126/science.1081311))
- Bercovici, D. & Karato, S. 2003 Whole-mantle convection and the transition-zone water filter. *Nature* **425**, 39–44. ([doi:10.1038/nature01918](https://doi.org/10.1038/nature01918))
- Cammarano, F. & Romanowicz, B. 2007 Insights into the nature of the transition zone from physically constrained inversion of long-period seismic data. *Proc. Natl Acad. Sci. USA* **104**, 9139–9144. ([doi:10.1073/pnas.0608075104](https://doi.org/10.1073/pnas.0608075104))
- Car, R. & Parrinello, M. 1985 Unified approach for molecular dynamics and density functional theory. *Phys. Rev. Lett.* **55**, 2471–2474. ([doi:10.1103/PhysRevLett.55.2471](https://doi.org/10.1103/PhysRevLett.55.2471))
- Caracas, R. & Cohen, R. E. 2005 Effect of chemistry on the stability and elasticity of the perovskite and post-perovskite phases in the MgSiO_3 – FeSiO_3 – Al_2O_3 system and implications for the lowermost mantle. *Geophys. Res. Lett.* **32**, L16 310. ([doi:10.1029/2005GL023164](https://doi.org/10.1029/2005GL023164))
- Carrez, P., Ferre, D. & Cordier, P. 2007 Peierls–Nabarro model for dislocations in MgSiO_3 post-perovskite calculated at 120 GPa from first principles. *Philos. Mag.* **87**, 3229–3247. ([doi:10.1080/14786430701268914](https://doi.org/10.1080/14786430701268914))
- de Koker, N. P., Stixrude, L. & Karki, B. B. 2008 Thermodynamics, structure, dynamics, and freezing of Mg_2SiO_4 liquid at high pressure. *Geochim. Cosmochim. Acta* **72**, 1427–1441. ([doi:10.1016/j.gca.2007.12.019](https://doi.org/10.1016/j.gca.2007.12.019))
- Dingwell, D. B., Courtial, P., Giordano, D. & Nichols, A. R. L. 2004 Viscosity of peridotite liquid. *Earth Planet. Sci. Lett.* **226**, 127–138. ([doi:10.1016/j.epsl.2004.07.017](https://doi.org/10.1016/j.epsl.2004.07.017))
- Dobson, D. P. & Brodholt, J. P. 2005 Subducted banded iron formations as a source of ultralow-velocity zones at the core–mantle boundary. *Nature* **434**, 371–374. ([doi:10.1038/nature03430](https://doi.org/10.1038/nature03430))
- Duffy, T. S. 2005 Synchrotron facilities and the study of deep planetary interiors. *Rep. Prog. Phys.* **68**, 1811–1859. ([doi:10.1088/0034-4885/68/8/R03](https://doi.org/10.1088/0034-4885/68/8/R03))
- Duffy, T. S. & Ahrens, T. J. 1992a Lateral variation in lower mantle seismic velocities. In *High-pressure research in mineral physics: applications to Earth and planetary sciences* (eds Y. Syono & M. H. Manghnani), pp. 197–206. Tokyo, Japan: Terra Scientific.
- Duffy, T. S. & Ahrens, T. J. 1992b Sound velocities at high-pressure and temperature and their geophysical implications. *J. Geophys. Res.* **97**, 4503–4520. ([doi:10.1029/91JB02650](https://doi.org/10.1029/91JB02650))
- Duffy, T. S., Zha, C. S., Downs, R. T., Mao, H.-K. & Hemley, R. J. 1995 Elasticity of forsterite to 16 GPa and the composition of the upper mantle. *Nature* **378**, 170–173. ([doi:10.1038/378170a0](https://doi.org/10.1038/378170a0))
- Duffy, T. S., Shen, G., Heinz, D. L., Shu, J. F., Ma, Y., Mao, H.-K., Hemley, R. J. & Singh, A. K. 1999 Lattice strains in gold and rhenium under nonhydrostatic compression to 37 GPa. *Phys. Rev. B* **60**, 15 063–15 073. ([doi:10.1103/PhysRevB.60.15063](https://doi.org/10.1103/PhysRevB.60.15063))
- Fiquet, G., Dewaele, A., Andrault, D., Kunz, M. & Bihan, T. L. 2000 Thermoelastic properties and crystal structure of MgSiO_3 perovskite at lower mantle pressure and temperature conditions. *Geophys. Res. Lett.* **27**, 21–24. ([doi:10.1029/1999GL008397](https://doi.org/10.1029/1999GL008397))
- Funamori, N., Jeanloz, R., Miyajima, N. & Fujino, K. 2000 Mineral assemblages of basalt in the lower mantle. *J. Geophys. Res.* **105**, 26 037–26 043. ([doi:10.1029/2000JB900252](https://doi.org/10.1029/2000JB900252))
- Garnero, E. J. 2000 Heterogeneity of the lowermost mantle. *Annu. Rev. Earth Planet. Sci.* **28**, 509–537. ([doi:10.1146/annurev.earth.28.1.509](https://doi.org/10.1146/annurev.earth.28.1.509))
- Gillan, M. J., Alfe, D., Brodholt, J., Vocadlo, L. & Price, G. D. 2006 First-principles modelling of Earth and planetary materials at high pressures and temperatures. *Rep. Prog. Phys.* **69**, 2365–2441. ([doi:10.1088/0034-4885/69/8/R03](https://doi.org/10.1088/0034-4885/69/8/R03))
- Greenwood, R. C., Franchi, I. A., Jambon, A. & Buchanan, P. C. 2005 Widespread magma oceans on asteroidal bodies in the early Solar System. *Nature* **435**, 916–918. ([doi:10.1038/nature03612](https://doi.org/10.1038/nature03612))
- Guignot, N., Andrault, D., Morard, G., Bolfan-Casanova, N. & Mezouar, M. 2007 Thermoelastic properties of post-perovskite phase MgSiO_3 determined experimentally at core–mantle boundary P – T conditions. *Earth Planet. Sci. Lett.* **256**, 162–168. ([doi:10.1016/j.epsl.2007.01.025](https://doi.org/10.1016/j.epsl.2007.01.025))
- Hernlund, J. W., Thomas, C. & Tackley, P. J. 2005 A doubling of the post-perovskite phase boundary and structure of the Earth's lowermost mantle. *Nature* **434**, 882–886. ([doi:10.1038/nature03472](https://doi.org/10.1038/nature03472))

- Hirose, K. 2006 Postperovskite phase transition and its geophysical implications. *Rev. Geophys.* **44**, RG3 001. ([doi:10.1029/2005RG000186](https://doi.org/10.1029/2005RG000186))
- Hirose, K., Fei, Y. W., Ma, Y. Z. & Mao, H. K. 1999 The fate of subducted basaltic crust in the Earth's lower mantle. *Nature* **397**, 53–56. ([doi:10.1038/16225](https://doi.org/10.1038/16225))
- Hirose, K., Kawamura, K., Ohishi, Y., Tateno, S. & Sata, N. 2005 Stability and equation of state of MgGeO_3 post-perovskite phase. *Am. Mineral.* **90**, 262–265. ([doi:10.2138/am.2005.1702](https://doi.org/10.2138/am.2005.1702))
- Hirose, K., Takafuji, N., Fujino, K., Shieh, S. R. & Duffy, T. S. In press. Iron partitioning between perovskite and post-perovskite: a transmission electron microscope study. *Am. Mineral.*
- Hustoft, J., Catalli, K., Shim, S. H., Kubo, A., Prakapenka, V. B. & Kunz, M. 2008 Equation of state of NaMgF_3 postperovskite: implication for the seismic velocity changes in the D'' region. *Geophys. Res. Lett.* **35**, L10 309. ([doi:10.1029/2008GL034042](https://doi.org/10.1029/2008GL034042))
- Hutko, A. R., Lay, T., Revenaugh, J. & Garnero, E. J. 2008 Anticorrelated seismic velocity anomalies from post-perovskite in the lowermost mantle. *Science* **320**, 1070–1074. ([doi:10.1126/science.1155822](https://doi.org/10.1126/science.1155822))
- Irifune, T. & Ringwood, A. E. 1993 Phase transformations in subducted oceanic crust and buoyancy relationships at depths of 600–800 km in the mantle. *Earth Planet. Sci. Lett.* **117**, 101–110. ([doi:10.1016/0012-821X\(93\)90120-X](https://doi.org/10.1016/0012-821X(93)90120-X))
- Irifune, T. & Tsuchiya, T. 2007 Mineralogy of the Earth: phase transitions and mineralogy of the lower mantle. In *Treatise on geophysics*, vol. 2 (ed. G. Schubert), pp. 33–62. Amsterdam, The Netherlands: Elsevier.
- Jeanloz, R. 1991 Effects of phase transitions and possible compositional changes on the seismological structure near 650 km depth. *Geophys. Res. Lett.* **18**, 1743–1746. ([doi:10.1029/91GL01839](https://doi.org/10.1029/91GL01839))
- Karato, S. 1993 Importance of anelasticity in the interpretation of seismic tomography. *Geophys. Res. Lett.* **20**, 1623–1626. ([doi:10.1029/93GL01767](https://doi.org/10.1029/93GL01767))
- Karato, S.-I. & Karki, B. B. 2001 Origin of lateral variation of seismic wave velocities and density in the deep mantle. *J. Geophys. Res.* **106**, 21 771–21 783. ([doi:10.1029/2001JB000214](https://doi.org/10.1029/2001JB000214))
- Karki, B. B., Bhattacharai, D. & Stixrude, L. 2006a First-principles calculations of the structural, dynamical, and electronic properties of liquid MgO . *Phys. Rev. B* **73**, 104 205. ([doi:10.1103/PhysRevB.73.174208](https://doi.org/10.1103/PhysRevB.73.174208))
- Karki, B. B., Bhattacharai, D. & Stixrude, L. 2006b A first-principles computational framework for liquid mineral systems. *Comput. Mater. Continua* **3**, 107–117.
- Kellogg, L. H., Hager, B. H. & van der Hilst, R. D. 1999 Compositional stratification in the deep mantle. *Science* **283**, 1881–1884. ([doi:10.1126/science.283.5409.1881](https://doi.org/10.1126/science.283.5409.1881))
- Kendall, J.-M. 2000 Seismic anisotropy in the boundary layers of the mantle. In *Earth's deep interior: mineral physics and tomography from the atomic to the global scale* (eds S.-I. Karato, A. M. Forte, R. C. Liebermann, G. Masters & L. Stixrude), pp. 133–159. Washington, DC: AGU.
- Kennett, B. L. N., Engdahl, E. R. & Buland, R. 1995 Constraints on seismic velocities in the Earth from travel times. *Geophys. J. Int.* **122**, 108–124. ([doi:10.1111/j.1365-246X.1995.tb03540.x](https://doi.org/10.1111/j.1365-246X.1995.tb03540.x))
- Kesson, S. E., Fitz Gerald, J. D. & Shelley, J. M. 1998 Mineralogy and dynamics of a pyrolite lower mantle. *Nature* **393**, 252–255. ([doi:10.1038/30466](https://doi.org/10.1038/30466))
- Komabayashi, T., Hirose, K., Sugimura, E., Sata, N., Ohishi, Y. & Dubrovinsky, L. S. 2008 Simultaneous volume measurements of post-perovskite and perovskite in MgSiO_3 and their thermal equations of state. *Earth Planet. Sci. Lett.* **265**, 515–524. ([doi:10.1016/j.epsl.2007.10.036](https://doi.org/10.1016/j.epsl.2007.10.036))
- Kubo, A., Kiefer, B., Shen, G. Y., Prakapenka, V. B., Cava, R. J. & Duffy, T. S. 2006 Stability and equation of state of the post-perovskite phase in MgGeO_3 to 2 Mbar. *Geophys. Res. Lett.* **33**, L12512. ([doi:10.1029/2006GL025686](https://doi.org/10.1029/2006GL025686))
- Kubo, A., Duffy, T. S., Shen, G. & Prakapenka, V. 2007 Stability and equation of state of post-perovskite phase in the system $\text{MgSiO}_3\text{--Al}_2\text{O}_3$ to 2 Mbar. *EOS Trans. AGU Fall Meeting Suppl.*, MR23D-07.
- Kubo, A., Kiefer, B., Shim, S.-H., Shen, G., Prakapenka, V. B. & Duffy, T. S. 2008 Rietveld structure refinements of MgGeO_3 post-perovskite phase to 1 Mbar. *Am. Mineral.* **93**, 965–976. ([doi:10.2138/am.2008.2691](https://doi.org/10.2138/am.2008.2691))

- Labrosse, S., Hernlund, J. W. & Coltice, N. 2007 A crystallizing dense magma ocean at the base of the Earth's mantle. *Nature* **450**, 866–869. ([doi:10.1038/nature06355](https://doi.org/10.1038/nature06355))
- Lacks, D. J., Rear, D. B. & Van Orman, J. A. 2007 Molecular dynamics investigation of viscosity, chemical diffusivities and partial molar volumes of liquids along the MgO–SiO₂ join as functions of pressure. *Geochim. Cosmochim. Acta* **71**, 1312–1323. ([doi:10.1016/j.gca.2006.11.030](https://doi.org/10.1016/j.gca.2006.11.030))
- Lay, T. & Garnero, E. J. 2007 Reconciling the post-perovskite phase with seismological observations of lowermost mantle structure. In *Post perovskite: the last mantle phase transition* (eds K. Hirose, J. P. Brodholt, T. Lay & D. A. Yuen), pp. 129–154. Washington, DC: AGU.
- Lay, T., Garnero, E. J. & William, Q. 2004 Partial melting in a thermo-chemical boundary layer at the base of the mantle. *Phys. Earth Planet. Inter.* **146**, 441–467. ([doi:10.1016/j.pepi.2004.04.004](https://doi.org/10.1016/j.pepi.2004.04.004))
- Lay, T., Hernlund, J., Garnero, E. J. & Thorne, M. S. 2006 A post-perovskite lens and D'' heat flux beneath the central Pacific. *Science* **314**, 1272–1276. ([doi:10.1126/science.1133280](https://doi.org/10.1126/science.1133280))
- Lee, K. K. M., O'Neill, B., Panero, W. R., Shim, S. H., Benedetti, L. R. & Jeanloz, R. 2004 Equations of state of the high-pressure phases of a natural peridotite and implications for the Earth's lower mantle. *Earth Planet. Sci. Lett.* **223**, 381–393. ([doi:10.1016/j.epsl.2004.04.033](https://doi.org/10.1016/j.epsl.2004.04.033))
- Liebske, C., Schmickler, B., Terasaki, H., Poe, B. T., Suzuki, A., Funakoshi, K., Ando, R. & Rubie, D. C. 2005 Viscosity of peridotite liquid up to 13 GPa: implications for magma ocean viscosities. *Earth Planet. Sci. Lett.* **240**, 589–604. ([doi:10.1016/j.epsl.2005.10.004](https://doi.org/10.1016/j.epsl.2005.10.004))
- Long, M. D., Xiao, X. H., Jiang, Z. T., Evans, B. & Karato, S. 2006 Lattice preferred orientation in deformed polycrystalline (Mg,Fe)O and implications for seismic anisotropy in D''. *Phys. Earth Planet. Inter.* **156**, 75–88. ([doi:10.1016/j.pepi.2006.02.006](https://doi.org/10.1016/j.pepi.2006.02.006))
- Mao, W. L., Shen, G. Y., Prakapenka, V. B., Meng, Y., Campbell, A. J., Heinz, D. L., Shu, J. F., Hemley, R. J. & Mao, H. K. 2004 Ferromagnesian postperovskite silicates in the D'' layer of the Earth. *Proc. Natl Acad. Sci. USA* **101**, 15 867–15 869. ([doi:10.1073/pnas.0407135101](https://doi.org/10.1073/pnas.0407135101))
- Mao, W. L., Mao, H. K., Prakapenka, V. B., Shu, J. F. & Hemley, R. J. 2006 The effect of pressure on the structure and volume of ferromagnesian post-perovskite. *Geophys. Res. Lett.* **33**, L12S02. ([doi:10.1029/2006GL025770](https://doi.org/10.1029/2006GL025770))
- Martin, C. D., Crichton, W. A., Liu, H. Z., Prakapenka, V., Chen, J. H. & Parise, J. B. 2006 Rietveld structure refinement of perovskite and post-perovskite phases of NaMgF₃ (neighborite) at high pressures. *Am. Mineral.* **91**, 1703–1706. ([doi:10.2138/am.2006.2308](https://doi.org/10.2138/am.2006.2308))
- Martin, C. D., Chapman, K. W., Chupas, P. J., Prakapenka, V., Lee, P. L., Shastri, S. D. & Parise, J. B. 2007 Compression, thermal expansion, structure, and instability of CaIrO₃, the structure model of MgSiO₃ post-perovskite. *Am. Mineral.* **92**, 1048–1053. ([doi:10.2138/am.2007.2473](https://doi.org/10.2138/am.2007.2473))
- Matsukage, K. N., Jing, Z. C. & Karato, S. 2005 Density of hydrous silicate melt at the conditions of Earth's deep upper mantle. *Nature* **438**, 488–491. ([doi:10.1038/nature04241](https://doi.org/10.1038/nature04241))
- McCammon, C. 2001 Geophysics—deep diamond mysteries. *Science* **293**, 813–814. ([doi:10.1126/science.1063295](https://doi.org/10.1126/science.1063295))
- McDonough, W. F. & Sun, S. S. 1995 The composition of the Earth. *Chem. Geol.* **120**, 223–253. ([doi:10.1016/0009-2541\(94\)00140-4](https://doi.org/10.1016/0009-2541(94)00140-4))
- Merkel, S., Kubo, A., Miyagi, L., Speziale, S., Duffy, T. S., Mao, H. K. & Wenk, H. R. 2006 Plastic deformation of MgGeO₃ post-perovskite at lower mantle pressures. *Science* **311**, 644–646. ([doi:10.1126/science.1121808](https://doi.org/10.1126/science.1121808))
- Merkel, S., McNamara, A. K., Kubo, A., Speziale, S., Miyagi, L., Meng, Y., Duffy, T. S. & Wenk, H. R. 2007 Deformation of (Mg,Fe)SiO₃ post-perovskite and D'' anisotropy. *Science* **316**, 1729–1732. ([doi:10.1126/science.1140609](https://doi.org/10.1126/science.1140609))
- Miller, G. H., Stolper, E. M. & Ahrens, T. J. 1991 The equation of state of a molten komatiite. 1. Shock-wave compression to 36 GPa. *J. Geophys. Res.* **96**, 11 831–11 848. ([doi:10.1029/91JB01204](https://doi.org/10.1029/91JB01204))
- Miyagi, L., Nishiyama, N., Wang, Y., Kubo, A., West, D. V., Cava, R. J., Duffy, T. S. & Wenk, H.-R. 2008 Deformation and texture development in CaIrO₃ post-perovskite phase up to 6 GPa and 1300 K. *Earth Planet. Sci. Lett.* **268**, 515–525. ([doi:10.1016/j.epsl.2008.02.005](https://doi.org/10.1016/j.epsl.2008.02.005))

- Miyajima, N., Ohgushi, K., Ichihara, M. & Yagi, T. 2006 Crystal morphology and dislocation microstructures of CaIrO₃: a TEM study of an analogue of the MgSiO₃ post-perovskite phase. *Geophys. Res. Lett.* **33**, L12302. ([doi:10.1029/2005GL025001](https://doi.org/10.1029/2005GL025001))
- Montelli, R., Nolet, G., Dahlen, F. A., Masters, G., Engdahl, E. R. & Hung, S. H. 2004 Finite-frequency tomography reveals a variety of plumes in the mantle. *Science* **303**, 338–343. ([doi:10.1126/science.1092485](https://doi.org/10.1126/science.1092485))
- Mosenfelder, J. L., Asimow, P. D. & Ahrens, T. J. 2007 Thermodynamic properties of Mg₂SiO₄ liquid at ultra-high pressures from shock measurements to 200 GPa on forsterite and wadsleyite. *J. Geophys. Res.* **112**, B06 208. ([doi:10.1029/2006JB004364](https://doi.org/10.1029/2006JB004364))
- Murakami, M., Hirose, K., Kawamura, K., Sata, N. & Ohishi, Y. 2004 Post-perovskite phase transition in MgSiO₃. *Science* **304**, 855–858. ([doi:10.1126/science.1095932](https://doi.org/10.1126/science.1095932))
- Oganov, A. R. & Ono, S. 2004 Theoretical and experimental evidence for a post-perovskite phase of MgSiO₃ in Earth's D'' layer. *Nature* **430**, 445–448. ([doi:10.1038/nature02701](https://doi.org/10.1038/nature02701))
- Oganov, A. R., Martonak, R., Laio, A., Raither, P. & Parrinello, M. 2005 Anisotropy of Earth's D'' layer and stacking faults in the MgSiO₃ post-perovskite phase. *Nature* **438**, 1142–1144. ([doi:10.1038/nature04439](https://doi.org/10.1038/nature04439))
- Ohtani, E. 1985 The primordial terrestrial magma ocean and its implication for stratification of the mantle. *Phys. Earth Planet. Inter.* **38**, 70–80. ([doi:10.1016/0031-9201\(85\)90123-2](https://doi.org/10.1016/0031-9201(85)90123-2))
- Ohtani, E. & Maeda, M. 2001 Density of basaltic melt at high pressure and stability of the melt at the base of the lower mantle. *Earth Planet. Sci. Lett.* **193**, 69–75. ([doi:10.1016/S0012-821X\(01\)00505-2](https://doi.org/10.1016/S0012-821X(01)00505-2))
- Ono, S. & Oganov, A. R. 2005 *In situ* observations of phase transition between perovskite and CaIrO₃-type phase in MgSiO₃ and pyrolytic mantle composition. *Earth Planet. Sci. Lett.* **236**, 914–932. ([doi:10.1016/j.epsl.2005.06.001](https://doi.org/10.1016/j.epsl.2005.06.001))
- Ono, S. & Ohishi, Y. 2005 *In situ* X-ray observation of phase transformation in Fe₂O₃ at high pressures and high temperatures. *J. Phys. Chem. Solids* **66**, 1714–1720. ([doi:10.1016/j.jpcs.2005.06.010](https://doi.org/10.1016/j.jpcs.2005.06.010))
- Ono, S., Kikegawa, T. & Ohishi, Y. 2006 Equation of state of CaIrO₃-type MgSiO₃ up to 144 GPa. *Am. Mineral.* **91**, 475–478. ([doi:10.2138/am.2006.2118](https://doi.org/10.2138/am.2006.2118))
- Prakapenka, V. B., Dubrovinsky, L. S., Shen, G., Rivers, M. L., Sutton, S. R., Dmitriev, V., Weber, H. P. & Le Bihan, T. 2003 α -PbO₂-type high-pressure polymorph of GeO₂. *Phys. Rev. B* **67**, 132 101. ([doi:10.1103/PhysRevB.67.132101](https://doi.org/10.1103/PhysRevB.67.132101))
- Reid, J. E., Poe, B. T., Rubie, D. C., Zotov, N. & Wiedenbeck, M. 2001 The self-diffusion of silicon and oxygen in diopside (CaMgSi₂O₆) liquid up to 15 GPa. *Chem. Geol.* **174**, 77–86. ([doi:10.1016/S0009-2541\(00\)00308-9](https://doi.org/10.1016/S0009-2541(00)00308-9))
- Reid, J. E., Suzuki, A., Funakoshi, K. I., Terasaki, H., Poe, B. T., Rubie, D. C. & Ohtani, E. 2003 The viscosity of CaMgSi₂O₆ liquid at pressures up to 13 GPa. *Phys. Earth Planet. Inter.* **139**, 45–54. ([doi:10.1016/S0031-9201\(03\)00143-2](https://doi.org/10.1016/S0031-9201(03)00143-2))
- Revenaugh, J. & Sipkin, S. A. 1994 Seismic evidence for silicate melt atop the 410 km mantle discontinuity. *Nature* **369**, 474–476. ([doi:10.1038/369474a0](https://doi.org/10.1038/369474a0))
- Rigden, S. M., Ahrens, T. J. & Stolper, E. M. 1984 Densities of liquid silicates at high pressures. *Science* **226**, 1071–1074. ([doi:10.1126/science.226.4678.1071](https://doi.org/10.1126/science.226.4678.1071))
- Righter, K. & Drake, M. J. 1996 Core formation in Earth's Moon, Mars, and Vesta. *Icarus* **124**, 513–529. ([doi:10.1006/icar.1996.0227](https://doi.org/10.1006/icar.1996.0227))
- Ringwood, A. E. 1991 Phase transformations and their bearing on the constitution and dynamics of the mantle. *Geochim. Cosmochim. Acta* **55**, 2083–2110. ([doi:10.1016/0016-7037\(91\)90090-R](https://doi.org/10.1016/0016-7037(91)90090-R))
- Ringwood, A. E. & Seabrook, M. 1963 High-pressure phase transformations in germanate pyroxenes and related compounds. *J. Geophys. Res.* **68**, 4601–4609. ([doi:10.1029/JZ068i004p01141](https://doi.org/10.1029/JZ068i004p01141))
- Rodi, F. & Babel, D. 1965 Ternare oxide der ubergangsmetalle 4. Erdalkaliiridium(4)-oxide—kristallstruktur von CaIrO₃. *Z. Anorg. Alleg. Chem.* **336**, 17–23. ([doi:10.1002/zaac.19653360104](https://doi.org/10.1002/zaac.19653360104))
- Romanowicz, B. 1991 Seismic tomography of the Earth's mantle. *Annu. Rev. Earth Planet. Sci.* **19**, 77–99. ([doi:10.1146/annurev.ea.19.050191.000453](https://doi.org/10.1146/annurev.ea.19.050191.000453))

- Ross, N. L. & Hazen, R. M. 1990 High-pressure crystal chemistry of MgSiO_3 perovskite. *Phys. Chem. Miner.* **17**, 228–237. ([doi:10.1007/BF00201454](https://doi.org/10.1007/BF00201454))
- Santillan, J., Shim, S. H., Shen, G. Y. & Prakapenka, V. B. 2006 High-pressure phase transition in Mn_2O_3 : application for the crystal structure and preferred orientation of the CaIrO_3 type. *Geophys. Res. Lett.* **33**, L15307. ([doi:10.1029/2006GL026423](https://doi.org/10.1029/2006GL026423))
- Sasaki, S., Prewitt, C. T. & Liebermann, R. C. 1983 The crystal structure of CaGeO_3 perovskite and the crystal chemistry of the GdFeO_3 -type perovskites. *Am. Mineral.* **68**, 1189–1198.
- Shieh, S. R., Duffy, T. S., Kubo, A., Shen, G. Y., Prakapenka, V. B., Sata, N., Hirose, K. & Ohishi, Y. 2006 Equation of state of the postperovskite phase synthesized from a natural $(\text{Mg}, \text{Fe})\text{SiO}_3$ orthopyroxene. *Proc. Natl Acad. Sci. USA* **103**, 3039–3043. ([doi:10.1073/pnas.0506811103](https://doi.org/10.1073/pnas.0506811103))
- Shim, S. H. 2008 The postperovskite transition. *Annu. Rev. Earth Planet. Sci.* **36**, 569–599. ([doi:10.1146/annurev.earth.36.031207.124309](https://doi.org/10.1146/annurev.earth.36.031207.124309))
- Shim, S. H., Catalli, K., Hustoft, J., Kubo, A., Prakapenka, V. B., Caldwell, W. A. & Kunz, M. 2008 Crystal structure and thermoelastic properties of $(\text{Mg}_{0.91}\text{Fe}_{0.09})\text{SiO}_3$ postperovskite up to 135 GPa and 2,700 K. *Proc. Natl Acad. Sci. USA* **105**, 7382–7386. ([doi:10.1073/pnas.0711174105](https://doi.org/10.1073/pnas.0711174105))
- Shiraki, K., Tsuchiya, T. & Ono, S. 2003 Structural refinements of high-pressure phases in germanium dioxide. *Acta Cryst. B* **59**, 701–708. ([doi:10.1107/S0108768103021761](https://doi.org/10.1107/S0108768103021761))
- Sidorin, I., Gurnis, M. & Helmberger, D. V. 1999 Evidence for a ubiquitous seismic discontinuity at the base of the mantle. *Science* **286**, 1326–1331. ([doi:10.1126/science.286.5443.1326](https://doi.org/10.1126/science.286.5443.1326))
- Solomatov, V. S. 2000 Fluid dynamics of a terrestrial magma ocean. In *Origin of the Earth and Moon* (eds R. M. Canup & K. Righter), pp. 323–338. Tucson, AZ: University of AZ Press.
- Song, T. R. A., Helmberger, D. V. & Grand, S. P. 2004 Low-velocity zone atop the 410-km seismic discontinuity in the northwestern United States. *Nature* **427**, 530–533. ([doi:10.1038/nature02231](https://doi.org/10.1038/nature02231))
- Stachel, T., Brey, G. P. & Harris, J. W. 2000 Kankan diamonds (Guinea) I: from the lithosphere down to the transition zone. *Contrib. Mineral. Petrol.* **140**, 1–15. ([doi:10.1007/s004100000173](https://doi.org/10.1007/s004100000173))
- Stackhouse, S. & Brodholt, J. P. 2007 The high-temperature elasticity of MgSiO_3 post-perovskite. In *Post perovskite: the last mantle phase transition* (eds K. Hirose, J. P. Brodholt, T. Lay & D. A. Yuen), pp. 99–113. Washington, DC: AGU.
- Stackhouse, S., Brodholt, J. P. & Price, G. D. 2005a High temperature elastic anisotropy of the perovskite and post-perovskite Al_2O_3 . *Geophys. Res. Lett.* **32**, L13 305. ([doi:10.1029/2005GL023163](https://doi.org/10.1029/2005GL023163))
- Stackhouse, S., Brodholt, J. P., Wookey, J., Kendall, J. M. & Price, G. D. 2005b The effect of temperature on the seismic anisotropy of the perovskite and post-perovskite polymorphs of MgSiO_3 . *Earth Planet. Sci. Lett.* **230**, 1–10. ([doi:10.1016/j.epsl.2004.11.021](https://doi.org/10.1016/j.epsl.2004.11.021))
- Stackhouse, S., Brodholt, J. P. & Price, G. D. 2006 Elastic anisotropy of FeSiO_3 end-members of the perovskite and post-perovskite phases. *Geophys. Res. Lett.* **33**, L01 304. ([doi:10.1029/2005GL023887](https://doi.org/10.1029/2005GL023887))
- Stixrude, L. & Karki, B. 2005 Structure and freezing of MgSiO_3 liquid in Earth's lower mantle. *Science* **310**, 297–299. ([doi:10.1126/science.1116952](https://doi.org/10.1126/science.1116952))
- Tateno, S., Hirose, K., Sata, N. & Ohishi, Y. 2005 Phase relations in $\text{Mg}_3\text{Al}_2\text{Si}_3\text{O}_{12}$ to 180 GPa: effect of Al on post-perovskite phase transition. *Geophys. Res. Lett.* **32**, L15 306. ([doi:10.1029/2005GL023309](https://doi.org/10.1029/2005GL023309))
- Tonks, W. B. & Melosh, H. J. 1993 Magma ocean formation due to giant impacts. *J. Geophys. Res.* **98**, 5319–5333. ([doi:10.1029/92JE02726](https://doi.org/10.1029/92JE02726))
- Tsuchiya, T. & Tsuchiya, J. 2007a High-pressure high-temperature phase relations of MgGeO_3 : first-principles calculations. *Phys. Rev. B* **76**, 092 105. ([doi:10.1103/PhysRevB.76.092105](https://doi.org/10.1103/PhysRevB.76.092105))
- Tsuchiya, T. & Tsuchiya, J. 2007b Structure and elasticity of Cmcm CaIrO_3 and their pressure dependences: *ab initio* calculations. *Phys. Rev. B* **76**, 144 119. ([doi:10.1103/PhysRevB.76.144119](https://doi.org/10.1103/PhysRevB.76.144119))
- Tsuchiya, T., Tsuchiya, J., Umemoto, K. & Wentzcovitch, R. A. 2004 Phase transition in MgSiO_3 perovskite in the Earth's lower mantle. *Earth Planet. Sci. Lett.* **224**, 241–248. ([doi:10.1016/j.epsl.2004.05.017](https://doi.org/10.1016/j.epsl.2004.05.017))

- Umemoto, K., Wentzcovitch, R. M., Weidner, D. J. & Parise, J. B. 2006 NaMgF₃: a low-pressure analog of MgSiO₃. *Geophys. Res. Lett.* **33**, L15 304. ([doi:10.1029/2006GL026348](https://doi.org/10.1029/2006GL026348))
- van der Hilst, R. D. & Karason, H. 1999 Compositional heterogeneity in the bottom 1000 kilometers of Earth's mantle: toward a hybrid convection model. *Science* **283**, 1885–1888. ([doi:10.1126/science.283.5409.1885](https://doi.org/10.1126/science.283.5409.1885))
- van der Hilst, R. D., Widjiantoro, S. & Engdahl, E. R. 1997 Evidence for deep mantle circulation from global tomography. *Nature* **386**, 578–584. ([doi:10.1038/386578a0](https://doi.org/10.1038/386578a0))
- van der Hilst, R. D., de Hoop, M. V., Wang, P., Shim, S. H., Ma, P. & Tenorio, L. 2007 Seismostratigraphy and thermal structure of Earth's core–mantle boundary region. *Science* **315**, 1813–1817. ([doi:10.1126/science.1137867](https://doi.org/10.1126/science.1137867))
- van Keken, P. E., Hauri, E. H. & Ballentine, C. J. 2002 Mantle mixing: the generation, preservation, and destruction of chemical heterogeneity. *Annu. Rev. Earth Planet. Sci.* **30**, 493–525. ([doi:10.1146/annurev.earth.30.091201.141236](https://doi.org/10.1146/annurev.earth.30.091201.141236))
- Walte, N., Heidelbach, F., Miyajima, N. & Frost, D. 2007 Texture development and TEM analysis of deformed CaIrO₃: implications for the D'' layer at the core–mantle boundary. *Geophys. Res. Lett.* **34**, L08 306. ([doi:10.1029/2007GL029407](https://doi.org/10.1029/2007GL029407))
- Wan, J. T. K., Duffy, T. S., Scandolo, S. & Car, R. 2007 First-principles study of density, viscosity, and diffusion coefficients of liquid MgSiO₃ at conditions of the Earth's deep mantle. *J. Geophys. Res.* **112**, B03 208. ([doi:10.1029/2005JB004135](https://doi.org/10.1029/2005JB004135))
- Warren, P. H. 1985 The magma ocean concept and lunar evolution. *Annu. Rev. Earth Planet. Sci.* **13**, 201–240. ([doi:10.1146/annurev.ea.13.050185.001221](https://doi.org/10.1146/annurev.ea.13.050185.001221))
- Wasserman, E. A., Yuen, D. A. & Rustad, J. R. 1993 Molecular dynamics study of the transport properties of perovskite melts under high-temperature and pressure conditions. *Earth Planet. Sci. Lett.* **114**, 373–384. ([doi:10.1016/0012-821X\(93\)90037-A](https://doi.org/10.1016/0012-821X(93)90037-A))
- Wentzcovitch, R. M., Tsuchiya, T. & Tsuchiya, J. 2006 MgSiO₃ postperovskite at D'' conditions. *Proc. Natl Acad. Sci. USA* **103**, 543–546. ([doi:10.1073/pnas.0506879103](https://doi.org/10.1073/pnas.0506879103))
- Williams, Q. & Garnero, E. J. 1996 Seismic evidence for partial melt at the base of Earth's mantle. *Science* **273**, 1528–1530. ([doi:10.1126/science.273.5281.1528](https://doi.org/10.1126/science.273.5281.1528))
- Williams, Q., Revenaugh, J. & Garnero, E. 1998 A correlation between ultra-low basal velocities in the mantle and hot spots. *Science* **281**, 546–549. ([doi:10.1126/science.281.5376.546](https://doi.org/10.1126/science.281.5376.546))
- Wookey, J., Stackhouse, S., Kendall, J. M., Brodholt, J. & Price, G. D. 2005 Efficacy of the post-perovskite phase as an explanation for lowermost-mantle seismic properties. *Nature* **438**, 1004–1007. ([doi:10.1038/nature04345](https://doi.org/10.1038/nature04345))
- Yamazaki, D., Yoshino, T., Ohfuji, H., Ando, J. I. & Yoneda, A. 2006 Origin of seismic anisotropy in the D'' layer inferred from shear deformation experiments on post-perovskite phase. *Earth Planet. Sci. Lett.* **252**, 372–378. ([doi:10.1016/j.epsl.2006.10.004](https://doi.org/10.1016/j.epsl.2006.10.004))